Benchmarks

MaranStable has been mainly designed to numerically investigate thermocapillary-driven flows. The package has a wide spectrum of implemented features. Before verifying and/or validating each feature separately, a grid convergence test is carried out for the default mesh parameters of MaranStable.

1 Grid convergence

In Stojanovic et al. (2022), the grid convergence was proven for a vertical liquid bridge made of 2-cSt silicone oil (Prandtl number $\mathrm{Pr} = 28$) under gravity conditions by employing the default mesh of MaranStable. Here we aim at showing grid convergence for a liquid bridge made from 5-cSt silicone oil ($\mathrm{Pr} \approx 68$), where the boundary layers are known to be even thinner compared to the case of 2-cSt silicone oil (Canright, 1994; Kamotani and Ostrach, 1998). To that end, we carry out a linear stability analysis for experimental conditions that are planned for the space experiment JEREMI (Barmak et al., 2021) and compute the critical Reynolds number $\mathrm{Re}_c = \rho_0 \gamma_0 \Delta T_c d/\mu_0^2$ and the critical dimensionless frequency $\omega_c = \Im(\xi_c)\rho_0 d^2/\mu_0$ for various grids of different sizes, where ρ_0, μ_0 and γ_0 denote the density, the dynamic viscosity, and the negative linear surface-tension coefficient, respectively, all evaluated at the reference temperature $T = 25°\mathrm{C}$. ΔT is the temperature difference imposed between the two cylindrical support rods of the liquid bridge which are separated by the length d, and ξ is the complex eigenvalue returned by the linear stability analysis. As a result of the linear stability analysis, we obtain the critical temperature difference ΔT_c as the real and imaginary parts of the complex growth rate ξ_c of the most dangerous perturbation (see e.g. Stojanovic et al., 2022).

In fig. 1, the dependence of Re_c and ω_c is monitored as function of $N = \sqrt{N_{\mathrm{tot}}}$, where N_{tot} is the total number of finite volumes employed. For a second-order numerical scheme, the critical Reynolds number Re_c should scale $\sim N^{-2}$ for large N. However, the data deviate from a linear convergence, since the grid is not homogeneous and since it is refined differently in each coordinate direction. Critical data for the single-fluid model (SFM) are shown in fig. 1(a). Quadratic regression of the data (dashed lines) yields the extrapolated values $(\mathrm{Re}_c, \omega_c)^{\mathrm{extra}} = (755.26, 10.088)$, which deviate only by (0.25%, 0.04%) from the critical data $(\mathrm{Re}_c, \omega_c)^{N=219} = (753.35, 10.092)$ obtained on the grid using the default mesh parameters (full symbols). For the two-fluid model (TFM), the quadratically extrapolated data $(\mathrm{Re}_c, \omega_c)^{\mathrm{extra}} = (574.16, 8.723)$ deviate only by (0.39%, 0.11%) from the critical data $(\mathrm{Re}_c, \omega_c)^{N=325} = (571.91, 8.713)$ obtained on the default mesh (see fig. 1). Comparing the extrapolated values with the critical data obtained on the finest grid gives an error estimate of at most (0.06%, 0.01%) for both the SFM and TFM. However, since those meshes are numerically too expensive for quasi-continuous parameter variations, the default meshes are a good compromise between accuracy and efficiency. Nevertheless, the user has the possibility to further refine (or dilate) the mesh, if needed.

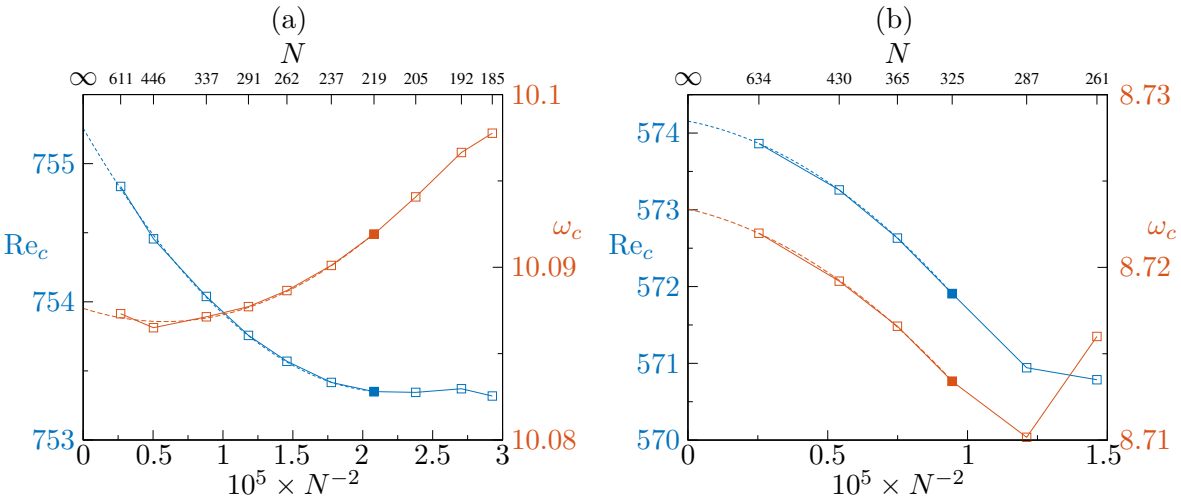

Figure 1: Critical Reynolds number Re_c (blue symbols) and critical frequency ω_c (red symbols) as functions of the grid size N for a liquid bridge made from 5-cSt silicone oil surrounded by argon under weightlessness conditions with aspect ratio $\Gamma = 0.66$ and volume ratio $\mathcal{V} = 1$. (a) Single-fluid model with an adiabatic free surface, disregarding viscous stresses in the gas phase. (b) Two-fluid model including the gas phase. The dashed lines in (a) and (b) indicate a quadratic regression using the finest grids up to the default grid (full symbols). The critical wave number is $m_c = 2$ for both models.

2 Code verification

In this section, we aim to verify the basic-state solver and the linear stability analysis based on the former. This is done separately for Cartesian coordinates and, thereafter, for cylindrical polar coordinates. For cylindrical coordinates, we als verify the handling of static and of dynamic interfacial deformations of the basic flow in case of a two-fluid system. Finally, the implementation of different flow models, distinguished by the treatment of the temperature dependence of the material parameters, is verified.

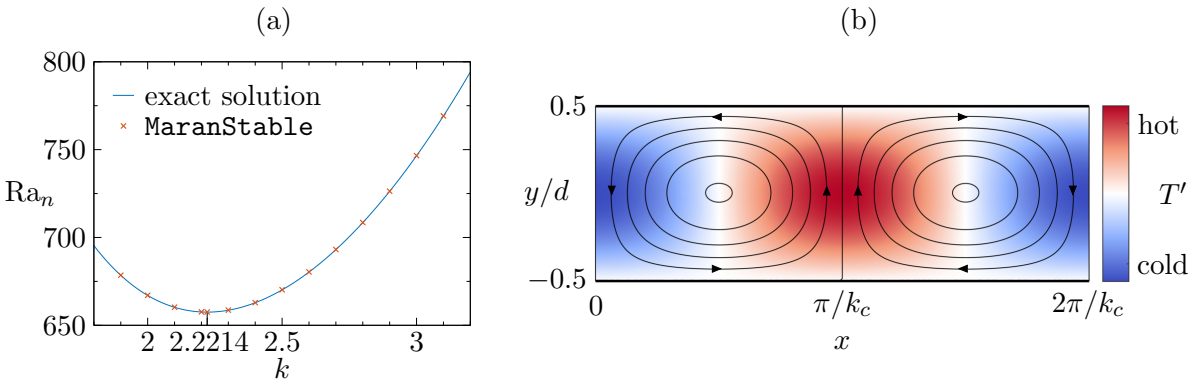

Figure 2: (a) Neutral curve for the Rayleigh-Bénard problem with free-slip conditions on the top and bottom boundaries; crosses: `MaranStable`, line: exact solution. (b) Streamlines and temperature field T' (color) of the critical mode ($k = k_c = 2.2214$).

2.1 Cartesian coordinates

To verify the linear stability solver for Cartesian coordinates, we consider the classic Rayleigh–Bénard problem (Rayleigh, Lord, 1916), i.e. the instability of the fluid at rest between two infinitely extended (in the x and z direction) parallel plates when the layer is heated from below. The single-fluid motion is governed by the NS1 approximation to the Navier–Stokes equations (Boussinesq approximation). We consider the case in which the horizontal top and bottom walls between which a temperature difference $\Delta T > 0$ is imposed are both free slip. The layer has a thickness of $d = 1\,\mathrm{mm}$ and the acceleration of gravity $\boldsymbol{g} = -g\boldsymbol{e}_y$ acts in the negative y direction. To mimic the infinitely extended system using a finite domain, we exploit the fact that convection between plane layers heated from below arises in form of two-dimensional stationary periodic counter-rotating rolls with rectangular cross-section and wavelength λ_c. Periodic boundary conditions in x direction suitable for plane layers are then equivalent to adiabatic free-slip conditions on the x boundaries of a rectangular Cartesian domain of length $L = \lambda_c$ in x direction.

For an infinite layer as well as for the surrogate rectangular box the basic flow is trivial: The fluid is at rest and the temperature varies linearly in y. If the length in x direction of the box $L = n\lambda_c/2$ equals an integer multiple of one half of the critical wave length of the infinite system, the critical temperature differences should be the same for both systems. Instead of the temperature difference the non-dimensional control parameter is the Rayleigh number $\mathrm{Ra} = g\beta\Delta T d^3\rho_0^2 c_{p0}/\mu_0\lambda_0$, where β, c_{p0} and λ_0 denote the constant, user-defined thermal expansion coefficient, specific heat capacity, and thermal conductivity, respectively.

Figure 2(a) shows the neutral Rayleigh number Ra_n, characterized by a vanishing growth rate, as function of the wave number in x direction. The exact solution for the infinitely extended system $\mathrm{Ra}_n^{\mathrm{exact}} = (k^2+\pi^2)^3/k^2$ (Rayleigh, Lord, 1916; Chandrasekhar, 1961) is shown as a full line. Results obtained by `MaranStable` are shown as red crosses. For the finite box used in `MaranStable` the wave number in x direction is $k = 2\pi/L$. `MaranStable` reproduces the exact solution up to 0.1% using a uniformly distributed grid with a total number of $N_{\mathrm{tot}} = 28300$ cells. The critical wave number k_c (minimum of Ra_n) found by `MaranStable` deviates by less than $10^{-4}\,\%$ from $k_c^{\mathrm{exact}} = \pi/\sqrt{2}$ (free–free boundary conditions). The critical mode obtained by `MaranStable` is shown in fig. 2(b).

2.2 Cylindrical coordinates

2.2.1 Basic flow

Cylindrical coordinates are typically employed to describe the flow in axisymmetric liquid bridges. Early numerical and theoretical analyses of thermocapillary flows in liquid bridges have neglected the gas phase using a single-fluid (SFM) model and assuming an adiabatic free surface (see e.g Wanschura et al., 1995). Particularly, the case of a length-to-radius aspect ratio $\Gamma = d/r_i = 1$ in combination with a volume ratio of $\mathcal{V} = V_{\mathrm{l}}/\pi r_i^2 d = 1$ has become a benchmark problem (Shevtsova, 2005). To verify the basic state solver, we compute the maximum absolute values of the non-dimensional Stokes stream function $\psi = \Psi\mu_0/d\gamma\Delta T$ arising in the bulk of a cylindrical liquid bridge with $\mathrm{Pr} = 4$ for different Reynolds numbers and grid resolutions and compare them with literature data (table 1). The data from `MaranStable` shown in table 1 are well

Table 1: Scaled maximum absolute value of the stream function $\tilde{\psi}_{\max} = \max|\psi| \times 10^3$ and relative (logarithmic) error $\delta\mathrm{Nu} = \sum_i \mathrm{Nu}_i / \max|\mathrm{Nu}_i|$ of the total Nusselt number for the thermocapillary flow in a cylindrical liquid bridge under weightlessness with $\Gamma = 1$, $\mathcal{V} = 1$, $\mathrm{Pr} = 4$, and an adiabatic free surface for different grid resolutions. Comparison is made with Ley: Leypoldt et al. (2000), Nien: Nienhüser (2002) and Rom: Romanò et al. (2017).

Grid/	Re = 3000		Re = 5000		Re = 7000	
Reference	$\tilde{\psi}_{\max}$	$\lg(\lvert\delta\mathrm{Nu}\rvert)$	$\tilde{\psi}_{\max}$	$\lg(\lvert\delta\mathrm{Nu}\rvert)$	$\tilde{\psi}_{\max}$	$\lg(\lvert\delta\mathrm{Nu}\rvert)$
121×121	2.1093	−12.3	2.0274	−12.2	1.9567	−12.4
160×160	2.1171	−12.2	2.0306	−12.2	1.9622	−12.4
260×260	2.1188	−13.1	2.0321	−12.9	1.9632	−12.5
360×360	2.1193	−12.3	2.0324	−12.3	1.9634	−12.4
Ley	2.09	—	1.97	—	1.86	—
Nien	—	—	2.03	−2.52	—	—
Rom	2.1783	—	2.0605	—	1.9735	—

converged. They deviate less than 3% from those for the highest resolution. Therefore, the values of the maximum stream function by `MaranStable` compare well with the literature data, for all resolutions used.

An additional test is the integral energy conservation. The total heat flux through the liquid bridge in non-dimensional form is

$$\sum_i \mathrm{Nu}_i = -\sum_i \int_{S_i} \boldsymbol{n}_i \cdot \nabla\vartheta \, \mathrm{d}S = 0, \tag{1}$$

where $\vartheta = (T - T_0)/\Delta T$ is the non-dimensional temperature and Nu_i is the Nusselt number that is assigned to each of the bounding surfaces, i.e. the hot and cold walls, and the free surface ($i \in [\mathrm{h}, \mathrm{c}, \mathrm{fs}]$). As a measurement for the accuracy of the energy preservation, we define the relative error as $\delta\mathrm{Nu} = \sum_i \mathrm{Nu}_i / \max|\mathrm{Nu}_i|$. Since the free surface is adiabatic in the cases considered in table 1, the corresponding heat flux vanishes, i.e. $\mathrm{Nu}_{\mathrm{fs}} = 0$. Thus, the heat flux through the hot wall must balance the one through the cold wall. As can be seen from table 1, the thermal energy of the basic state is conserved up to $\delta\mathrm{Nu} < 10^{-12}$ for all presented calculations. Employing a two-fluid model (TFM), for which the heat flux through the free surface does not vanish ($\mathrm{Nu}_{\mathrm{fs}} \neq 0$), we obtain the same order of magnitude of $\delta\mathrm{Nu}$ (not shown).

2.2.2 Linear stability analysis

The linear stability analysis is verified by considering the same benchmark of a cylindrical liquid bridge as in table 1 but for $\mathrm{Pr} = 4$ and $\mathrm{Pr} = 7$. Using the default mesh, the critical parameters Re_c and ω_c found by `MaranStable` deviate less than 1% from the data of Levenstam et al. (2001) and Carrión et al. (2020) for both Pr numbers (table 2). The somewhat larger deviation of Re_c by 2.8% with respect to the result of Shevtsova et al. (2001) could be related to their method of determining the critical onset by numerical simulation and by using a coarser mesh (25×21) in the (r, z) plane. Furthermore, the

Table 2: Critical data for common benchmarks (Pr = 4 and 7) for the linear stability of the flow in a cylindrical thermocapillary liquid bridge with Γ = 1, adiabatic free-surface, zero gravity, and negligible viscous stresses from the gas phase (SFM). Comparison is made with Wan: Wanschura et al. (1995), Shev: Shevtsova et al. (2001), Lev: Levenstam et al. (2001) and Car: Carrión et al. (2020). FV: finite volumes, FD: finite differences, FE: finite elements.

		Pr = 4		Pr = 7	
Authors	resolution	Re_c	ω_c	Re_c	ω_c
MaranStable	176 × 197 (FV)	1002	28.43	876	22.91
Wan	20 × 80 (spectral, FD)	1047	27.9	—	—
Shev	$(N_r, N_\varphi, N_z) = (25, 16, 21)$ (FV simulation)	1030	28.72	—	—
Lev	41 × 41 (FE)	1002	28.5	869	22.9
Car	91 × 91 (FD)	1000	28.45	—	—

deviation of 4.5% in Re_c from the result of Wanschura et al. (1995) for Pr = 4 can be explained by the regularization of the thermocapillary stresses within 10% of d from each corner employed by Wanschura et al. (1995) in order to overcome the corner singularity. Suppressing the driving force close to the hot and cold corners obviously leads to an more stable flow and, thus, to a larger critical Reynolds number as found by these authors.

2.2.3 Static and dynamic surface shapes

Three different approximations are implemented in MaranStable to treat the liquid–gas interface: straight indeformable surface shape (I1), indeformable hydrostatic surface shape (I2) and dynamically deformed surface shape (I3). Among these approaches, only I2 and I3 need to be verified. Approximation I2 represents the asymptotic limit of vanishing Capillary number $\mathrm{Ca} = \gamma \Delta T/\sigma_0 \to 0$, corresponding to an asymptotically large mean surface tension σ_0. In this limit, detecting the shape of the interface $h(z)$ decouples from solving the basic state equations and the normal stress balance reduces to the Young–Laplace equation (Stojanovic et al., 2022). Within I2, flow-induced (dynamic) surface deformations can be neglected. Thus, the *static* surface shape $h_\mathrm{s}(z)$ is known and only parametrically enters the interfacial boundary conditions for the basic velocity and temperature. To verify the static interfacial shape computed using the approach I2, we consider the zero gravity conditions. In this case the Young–Laplace equation has the closed-form solution of a catenoid (Kenmotsu, 1980; Langbein, 2002)

$$h_\mathrm{cat}(z) = h_0 \cosh\left(\frac{z}{h_0}\right) \quad \text{with} \quad h_0 \cosh\left(\frac{1}{2h_0}\right) = \frac{1}{\Gamma}. \tag{2}$$

Figure 3(a) compares the numerically computed shape of the interface with the catenoid profile for Γ = 1 and $h_0 = 0.848$. A second-order convergence is confirmed by fig. 3(b), where the L_2 and L_∞ norms of the deviation $\epsilon = h(z) - h_\mathrm{cat}(z)$ are monitored as

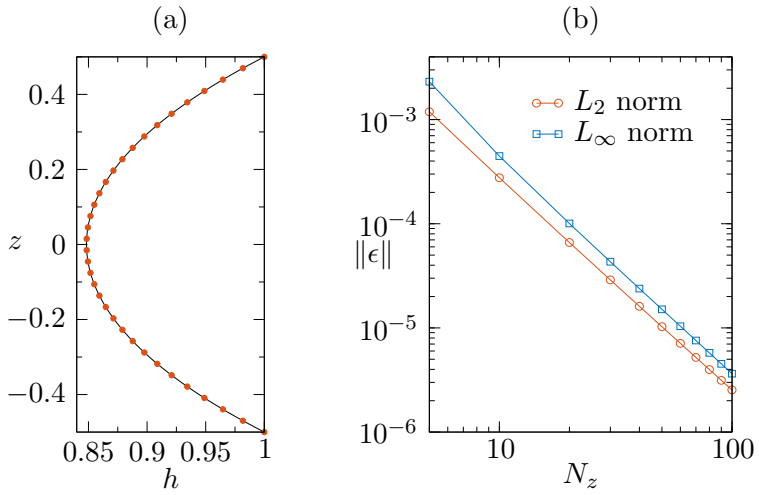

Figure 3: (a) Comparison of the catenoid profile $h_{\mathrm{cat}}(z)$ (line) according to (2) with the numerical solution $h(z)$ (red dots) of the Young–Laplace equation for $\Gamma = 1$ and $h_0 = 0.848$ using an equidistant grid with $N_z = 34$ grid points. (b) L_2- and L_∞-norms of the deviation $\epsilon(z) = h(z) - h_{\mathrm{cat}}(z)$ of the numerical solution from the exact catenoid as functions of the number of grid points N_z.

functions of the number of grid points N_z, uniformly distributed over the height of the liquid bridge.

While the interface within I2 is assumed to be statically deformed by the hydrostatic and the Laplace pressure, the more realistic model I3 allows the liquid–gas interface to be dynamically deformed, in particular, depending on the temperature and the velocity field. To this end, the transport equations are solved simultaneously for both, the liquid and the gas phase coupled by the full thermal and mechanical free-surface boundary conditions. Thus, within I3, the *dynamic* surface shape $h_{\mathrm{d}}(z)$ is part of the numerical solution. Note that also for the (SFM), dynamic surface deformations will arise despite of the neglected gas phase. To check the implementation of the dynamically deformed free-surface shape, we compare h_{d} obtained using approach I3 with the surface shape up to first order in Ca of an asymptotic expansion obtained by Kuhlmann and Nienhüser (2002). For a comparison with their result, we consider a liquid bridge under zero gravity within the (SFM) for $\Gamma = 1$, $\mathcal{V} = 1$, $\mathrm{Ca} = 10^{-6}$ and an adiabatic free surface. Under zero gravity, the static shape is cylindrical corresponding to $h_{\mathrm{s}}(z) \equiv 1/\Gamma$ in non-dimensional form. Figure 4 shows the deviation $\Delta h_{\mathrm{d}} - h_{\mathrm{s}}$ of the surface shape from cylindrical obtained by `MaranStable` (lines) in comparison with the first-order correction $h^{(1)}\mathrm{Ca}$ to the cylindrical shape computed by Kuhlmann and Nienhüser (2002) (dots) for different combinations of Re and Pr. Our results agree very well with the literature data, in particular for the viscous–conductive case $\mathrm{Re} = 10^{-4}$, $\mathrm{Pr} = 0.02$ (blue). Deviations among the two results slightly increase for larger Marangoni numbers $\mathrm{Ma} = \mathrm{RePr}$, i.e. for $\mathrm{Re} = 2130$, $\mathrm{Pr} = 0.02$ and for $\mathrm{Re} = 951$, $\mathrm{Pr} = 4.38$. A plausible reason for these minor deviations is the absence of higher-order corrections in Ca of interface shapes provided by Kuhlmann and Nienhüser (2002).

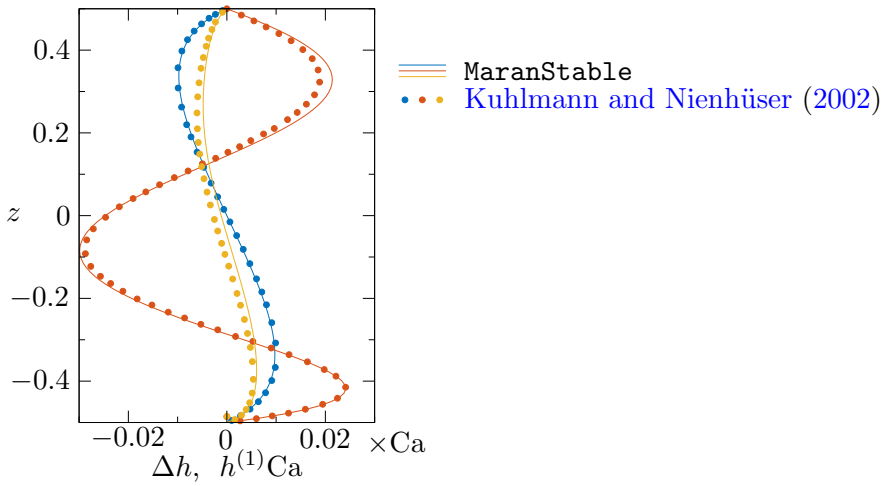

Figure 4: Comparison of the scaled dynamic surface deformations Δh (lines) with the first-order correction $h^{(1)}\mathrm{Ca}$ of Kuhlmann and Nienhüser (2002) (dots, taken from their fig. 2(a)) for $\Gamma = 1$, $\mathcal{V} = 1$, $\mathrm{Bd} = \mathrm{Bo} = 0$, $\mathrm{Ca} = 10^{-6}$, adiabatic free surface and $(\mathrm{Pr}, \mathrm{Re}) = (0.02, 10^{-4})$ (blue), $(0.02, 2130)$ (red) and $(4.38, 951)$ (yellow). Viscous stresses from the gas phase are neglected.

2.2.4 Temperature-dependent fluid properties

As pointed out in Stojanović et al. (n.d.), `MaranStable` implements three forms of transport equations for single- and immiscible multiphase flows, denoted NS1, NS2 and NS3. For the sake of simplicity, most previous numerical investigations on liquid bridges tackled the problem by assuming constant fluid properties except for surface tension. In the case of gravity forces, it is common to use the Oberbeck–Boussinesq approximation NS1. In contrast, `MaranStable` has the capability to either account for a linear (NS2) or the fully non-linear temperature dependence of all fluid properties (NS3).

For the verification of flow model NS2, we adopt the setup of Melnikov et al. (2002), where the viscosity $\mu(T) = \mu_0[1 - \alpha_\mu(T - T_0)]$ is assumed to be a linear function of the temperature. The remaining thermophysical properties ρ, λ and c_p are assumed to be constant. In fig. 5, a comparison is made between the critical data Re_c and ω_c obtained by `MaranStable` (circles) and Melnikov et al. (2002) (squares). Results are given as functions of the non-dimensional viscosity variation $R_\nu = -\alpha_\mu \Delta T$. A good agreement is found for all R_ν considered. The critical Reynolds numbers Re_c reported by Melnikov et al. (2002) (blue squares) are about 5% larger than those obtained by `MaranStable` (blue circles), but the slopes with respect to R_ν agree very well. The maximum deviation of 2% in ω_c is even smaller than for Re_c. The slightly higher critical Reynolds numbers found by Melnikov et al. (2002) might be related to their numerical treatment of the problem, using a three-dimensional time-dependent simulation rather than a stability analysis. Their mesh of 24×16 grid points in the (r, z) plane was much coarser than the one used in `MaranStable`. Furthermore, some regularization of the thermocapillary stresses near the hot and cold corners might have been applied, as was done by Wanschura et al. (1995).

We are not aware of numerical investigations taking into account the full temperature dependence of all thermophysical parameters. Therefore, the results obtained by

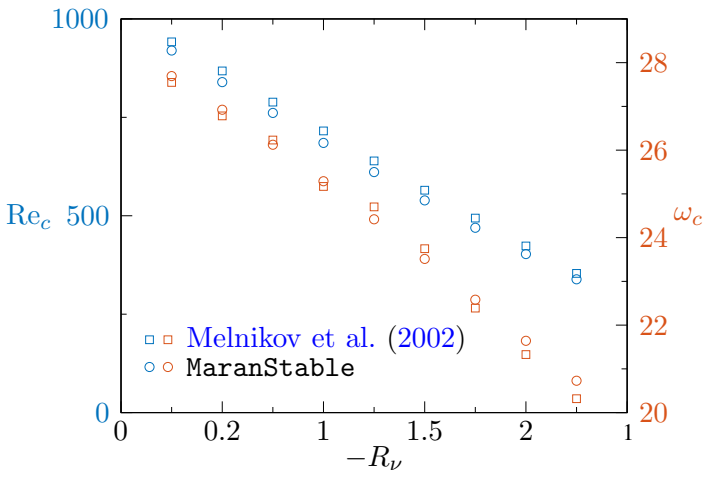

Figure 5: Critical Reynolds numbers Re_c (blue symbols) and critical oscillation frequencies ω_c (red symbols) as functions of the non-dimensional parameter $R_\nu = -\alpha_\mu \Delta T$ under weightlessness conditions with $\Gamma = 1$, $\mathcal{V} = 1$ and $\mathrm{Pr} = 4$. Squares: data taken from Melnikov et al. (2002); circles: results of `MaranStable`.

`MaranStable` using the flow model NS3 (red dots in fig. 6) are compared here with the result of the code of Romanò et al. (2017) (full line) who considered the full temperature dependence of the kinematic viscosity and the thermal diffusivity, of which the former typically varies the most. A comparison between the results of both codes for the basic-state temperature distribution T and the basic axial velocity w along the free surface is made in fig. 6 for representative parameters of the planned space experiment JEREMI (Barmak et al., 2021), i.e. $d = r_i = 5\,\mathrm{mm}$, $d_1 = d_2 = r_o = 15\,\mathrm{mm}$, $T_0 = 25°\mathrm{C}$, $\Delta T = 40\,\mathrm{K}$ and a closed gas tube. Both surface quantities, T and w, crucially affect the instability and depend on the flow in the liquid and the gas. The results of both codes agree up to the line's thickness, even when using different grid resolutions in the z direction. To demonstrate the significance of the flow model NS3, we also show the results for constant material properties (flow model NS1, blue dots). In view of the comparisons made in section 2 we consider `MaranStable` verified.

3 Code validation

To validate the static and dynamic surface shapes obtained by `MaranStable` we compare with the experimental results obtained by Matsunaga et al. (2012). The geometry of the experimental setup is governed by $d = r_i = 3\,\mathrm{mm}$, $d_1 = d_2 = 2\,\mathrm{mm}$ and $r_o = 5\,\mathrm{mm}$. The deviation $h_\mathrm{s} - 1/\Gamma$ of the non-dimensional static equilibrium shape h_s from the upright cylindrical shape $h = 1/\Gamma$ for the volume ratio $\mathcal{V} = 0.80$ (filling factor) under normal gravity conditions is shown in fig. 7(a). Matsunaga et al. (2012) themselves state that the measured hydrostatic surface profiles deviate less than 0.1% from the solution of the Young–Laplace equation.

In the experiments, the liquid bridge is isothermal and nitrogen gas enters from below ($\bar{w}_\mathrm{g} > 0$) through the annular inlet. Therefore, the dynamic surface deformations of the 5-cSt silicone oil liquid bridge are caused solely by the axisymmetric gas flow. The flow-

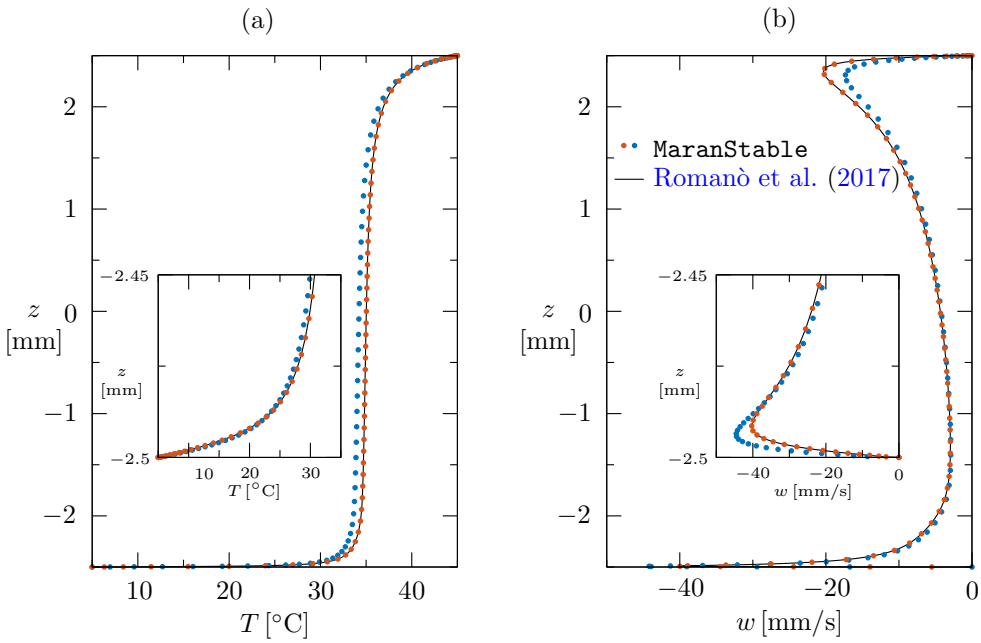

Figure 6: Comparison of the surface temperatures (a) and the axial surface velocities (b) of the steady axisymmetric basic flow in a thermocapillary liquid bridge for $d = r_i = 5\,\mathrm{mm}$, $d_1 = d_2 = r_o = 15\,\mathrm{mm}$, $T_0 = 25°\mathrm{C}$, $\Delta T = 40\,\mathrm{K}$, a closed gas tube and a straight indeformable interface. Solid line: Code of Romanò et al. (2017). Red dots: results of `MaranStable` using NS3. Blue dots: results of `MaranStable` using NS1.

induced contribution to the dynamic deformation $\Delta h = h_\mathrm{d} - h_\mathrm{s}$ is shown in fig. 7(b) for different mean inlet velocities. The profiles computed by `MaranStable` for $\bar{w}_\mathrm{g} = 1\,\mathrm{m/s}$ (blue line) and $\bar{w}_\mathrm{g} = 1.5\,\mathrm{m/s}$ (red line) are in excellent agreement with the corresponding experimental results (symbols). However, for $\bar{w}_\mathrm{g} = 2\,\mathrm{m/s}$ (yellow line), the deviations are considerably larger.

Dynamic surface deformations arise not only due to viscous shear stresses from the gas phase but also due to a temperature gradient along the interface. To validate the latter phenomenon, we compare our results with the measurements of Montanero et al. (2008). While the experimental data are obtained in the presence of the gas phase, it is neglected in our calculations. The reason is Montanero et al. (2008) did not provide any information about the ambient gas and the complimentary numerical computations by Carrión et al. (2020) also assumed a single-fluid model. Following Carrión et al. (2020) we assume the thermal boundary condition can be modeled by Newton's law of cooling

$$\boldsymbol{n} \cdot \nabla \vartheta = -\mathrm{Bi}\left(\vartheta + \frac{1}{2}\right), \tag{3}$$

with an ambient temperature corresponding to the cold-wall temperature and a Biot number $\mathrm{Bi} = h_q d/\lambda = 0.15$, where h_q is the heat-transfer coefficient between the liquid and the gas. We consider a liquid bridge of length $d = 3.691\,\mathrm{mm}$ made from 5-cSt silicone oil with $r_i = 3\,\mathrm{mm}$ and $\mathcal{V} = 0.82$ (underfilling) under normal gravity. Figure 8(a) shows the static surface shape computed using `MaranStable`. The horizontal axes show both the dimensional $(H_\mathrm{s} - r_i)$ and the non-dimensional deviation $(h_\mathrm{s} - 1/\Gamma)$ of the free surface position from cylindrical. The (additional) flow-induced dynamic deformation

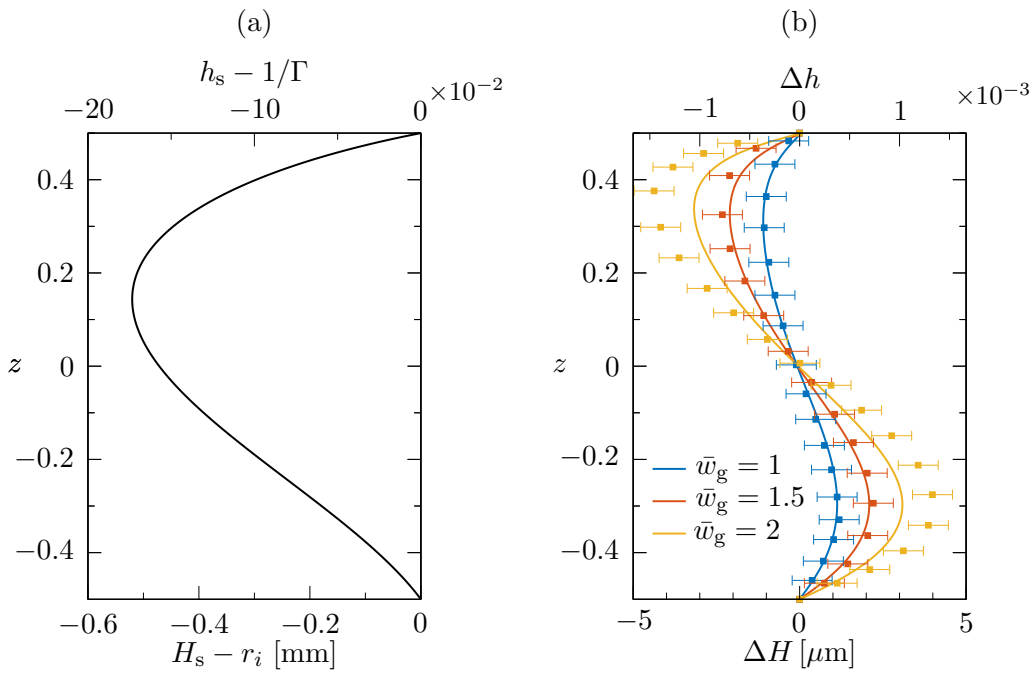

Figure 7: (a) Deviation $h_{0,s} - 1/\Gamma$ of the static interface shape from cylindrical for a liquid bridge of length $d = 3\,\text{mm}$ made from 5-cSt silicone oil in nitrogen. The essential non-dimensional parameters are: $\Gamma = 1$, $\mathcal{V} = 0.8$, $\text{Bo} = 4.075$ (normal gravity conditions) and $\text{Re} = 0$ (see the text for the remaining geometry parameters). (b) Dynamic part of the interfacial deformation Δh computed using `MaranStable` (lines) in comparison with the measurements of Matsunaga et al. (2012) (squares) for different mean gas flow velocities: $\bar{w}_g = 1\,\text{m/s}$ (blue), $\bar{w}_g = 1.5\,\text{m/s}$ (red) and $\bar{w}_{in} = 2\,\text{m/s}$ (yellow). Error bars show an uncertainty of $\pm 0.6\,\mu\text{m}$.

$\Delta h = h_d - h_s$ is shown in fig. 8(b). The results obtained with `MaranStable` show a reasonable agreement with the experimental data. Regardless of the measurement error, the remaining deviations are not surprising, because the heat flux through the interface is not correctly described by (3) when using a constant Biot number (Romanò and Kuhlmann, 2019).

Finally, we validate our linear stability analysis for the different physical models NS1–NS3 with the experimental data measured by Yano et al. (2016). To that end, we consider two liquid bridges of $d = r_i = 2.5\,\text{mm}$ made of 2-cSt and 5-cSt silicone oil, respectively, both surrounded by air. Figure 9 shows the neutral and critical Marangoni numbers as functions of the volume ratio $\mathcal{V}$, for a closed gas container (fig. 9(a)) and for an open gas tube (figs. 9(b,c)) with a hot vertically downward gas flow. Since the gas in Yano et al. (2016) enters the tube through a porous medium to achieve a uniform gas flow, we prescribe a constant gas velocity at the inlet of $w_g(r) \equiv \bar{w}_g = -35\,\text{mm/s}$. Considering the 2-cSt liquid bridge (fig. 9(a,b)), the numerical critical Marangoni numbers obtained with NS2 (dashed lines) and NS3 (full lines) agree very well with the experimental data within the experimental error bar for both, closed and open gas tubes. Merely for $\mathcal{V} = 1$ some deviations exist, because the slope of the critical curve for $m = 1$ with respect to $\mathcal{V}$ is very large. For moderate temperature differences ΔT the flow model NS1 is sufficient to predict the critical Marangoni number. However, for the largest measured ΔT in fig.

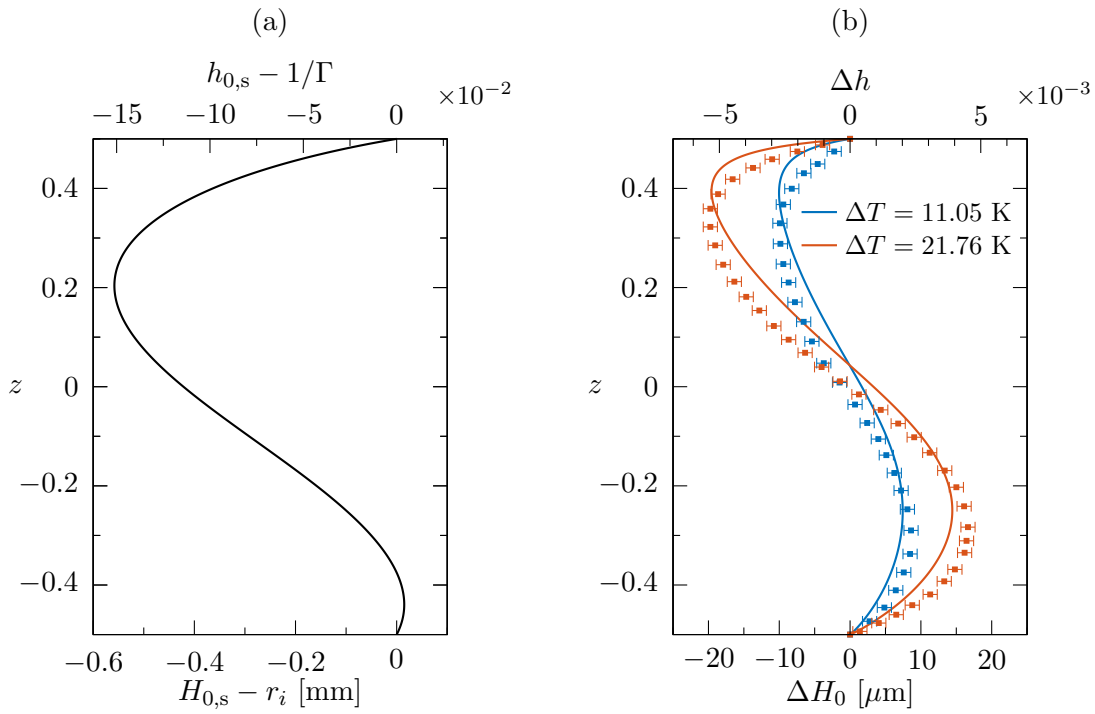

Figure 8: (a) Static surface shape h_s of a tall liquid bridge made from 5-cSt silicone oil under normal gravity with length $d = 3.691$ mm, radius $r_i = 3$ mm and volume $\mathcal{V} = 0.82$. (b) Dynamic surface deformation Δh for the same liquid bridge for $\Delta T = 11.05$ K (blue) and $\Delta T = 21.76$ K (red). Lines: results of `MaranStable`. Squares: experimental data of Montanero et al. (2008). The error bars indicate the inaccuracy of the measurement ($\pm 1\,\mu$m) estimated by Montanero et al. (2008).

9(a), i.e. $\Delta T \approx 27$°C for $\mathcal{V} = 0.95$, the Marangoni number predicted by NS1 would be too large.

For the 5-cSt liquid bridge the critical temperature difference are larger (see fig. 9(c)), resulting in larger deviations among the different flow models, even between NS2 and NS3. For $\mathcal{V} < 1$, NS3, being the most accurate model, yields the best predictions. However, for $\mathcal{V} \gtrsim 0.97$ NS3 predicts a critical mode with $m = 2$, where as $m = 1$ is found in the experiments. This indicates that certain influence factors are not accounted for within NS3. Possible candidates are evaporative cooling effects or experimental imperfections (a decentration could favor an $m = 1$ mode).

Despite of the relatively large experimental error bar and the differences between experiment and numerics for very large temperature differences, our code can be considered validated for small and moderate temperature differences (fig. 9(a,b)).

References

Barmak, I., Romanò, F. and Kuhlmann, H. C. (2021), 'Finite-size coherent particle structures in high-Prandtl-number liquid bridges', *Phys. Rev. Fluids* **6**, 084301 (36pp). **URL:** *https://link.aps.org/doi/10.1103/PhysRevFluids.6.084301*

Canright, D. (1994), 'Thermocapillary flow near a cold wall', *Phys. Fluids* **6**, 1415–1424.

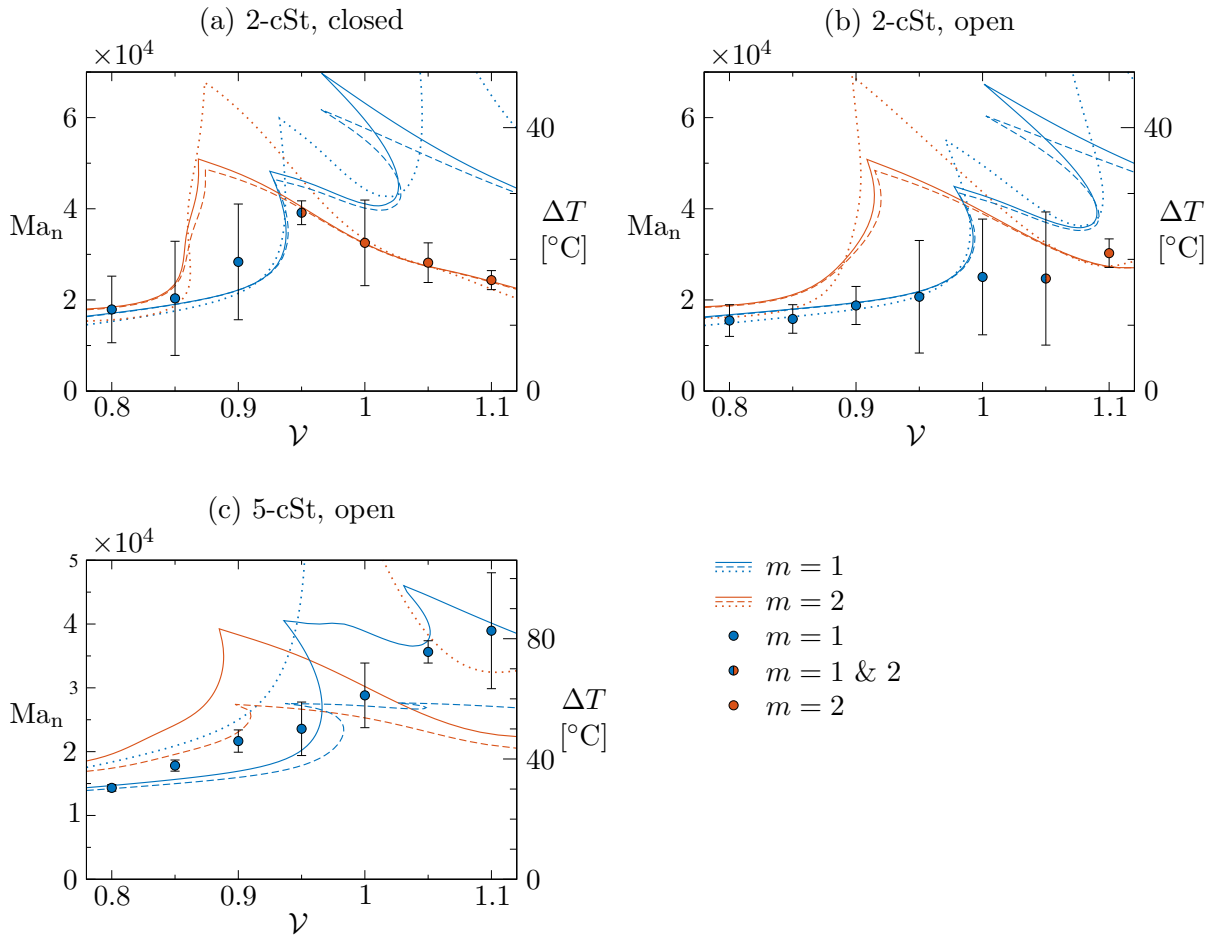

Figure 9: Neutral Marangoni numbers (lines) as functions of the volume ratio $\mathcal{V}$ for a liquid bridge of 2-cSt (a,b) and 5-cSt (c) silicone oil in air with $d = r_i = 2.5\,\text{mm}$, $d_1 = d_2 = 12\,\text{mm}$ and $r_o = 12.5\,\text{mm}$ under normal gravity conditions. The gas tube is closed in (a) and open in (b,c) with $\bar{w}_\text{g} = -35\,\text{mm/s}$. Full lines: NS3, dashed lines: NS2, dotted lines: NS1. A comparison is made with experimental data of Yano et al. (2016) (their figs. 6(a) and 6(b)). Color indicates the neutral wave number: $m = 1$ (blue) and $m = 2$ (red).

Carrión, L. M., Herrada, M. A. and Montanero, J. M. (2020), 'Influence of the dynamical free surface deformation on the stability of thermal convection in high-Prandtl-number liquid bridges', *Intl J. Heat Mass Transfer* **146**, 118831 (10pp).

Chandrasekhar, S. (1961), *Hydrodynamic and Hydromagnetic Stability*, Oxford University Press, Oxford.

Kamotani, Y. and Ostrach, S. (1998), 'Theoretical analysis of thermocapillary flow in cylindrical columns of high Prandtl number fluids', *ASME J. Heat Transfer* **120**, 758–764.

Kenmotsu, K. (1980), 'Surfaces of revolution with prescribed mean curvature', *Tôhoku Math. Journ.* **32**(1), 147–153.
URL: *https://doi.org/10.2748/tmj/1178229688*

Kuhlmann, H. C. and Nienhüser, C. (2002), 'Dynamic free-surface deformations in thermocapillary liquid bridges', *Fluid Dyn. Res.* **31**, 103–127.

Langbein, D. (2002), *Capillary surfaces: Shape – stability – dynamics, in particular under weightlessness*, Vol. 178 of *Springer Tracts in Modern Physics*, Springer, Berlin, Heidelberg.

Levenstam, M., Amberg, G. and Winkler, C. (2001), 'Instabilities of thermocapillary convection in a half-zone at intermediate Prandtl numbers', *Phys. Fluids* **13**, 807–816.

Leypoldt, J., Kuhlmann, H. C. and Rath, H. J. (2000), 'Three-dimensional numerical simulation of thermocapillary flows in cylindrical liquid bridges', *J. Fluid Mech.* **414**, 285–314.

Matsunaga, T., Mialdun, A., Nishino, K. and Shevtsova, V. (2012), 'Measurements of gas/oil free surface deformation caused by parallel gas flow', *Phys. Fluids* **24**(6), 062101 (17pp).

Melnikov, D. E., Shevtsova, V. M. and Legros, J. C. (2002), 'Numerical simulation of hydro-thermal waves in liquid bridges with variable viscosity', *Adv. Space Res.* **29**, 661–666.

Montanero, J. M., Ferrera, C. and Shevtsova, V. M. (2008), 'Experimental study of the free surface deformation due to thermal convection in liquid bridges', *Exp. Fluids* **45**, 1087–1101.

Nienhüser, C. (2002), Lineare Stabilität achsensymmetrischer thermokapillarer Konvektion in Flüssigkeitsbrücken mit statisch und dynamisch deformierbarer Grenzfläche, PhD thesis, Fachbereich Produktionstechnik.

Rayleigh, Lord (1916), 'On convection currents in a horizontal layer of fluid, when the higher temperature is on the under side', *Phil. Mag.* **32**, 529–546.

Romanò, F. and Kuhlmann, H. C. (2019), 'Heat transfer across the free surface of a thermocapillary liquid bridge', *Tech. Mech.* **39**, 72–84.

Romanò, F., Kuhlmann, H. C., Ishimura, M. and Ueno, I. (2017), 'Limit cycles for the motion of finite-size particles in axisymmetric thermocapillary flows in liquid bridges', *Phys. Fluids* **29**(9), 093303 (14pp).
URL: *http://dx.doi.org/10.1063/1.5002135*

Shevtsova, V. (2005), 'Thermal convection in liquid bridges with curved free surfaces: Benchmark of numerical solutions', *J. Crystal Growth* **280**, 632–651.

Shevtsova, V. M., Melnikov, D. E. and Legros, J. C. (2001), 'Three-dimensional simulations of hydrodynamic instability in liquid bridges: Influence of temperature-dependent viscosity', *Phys. Fluids* **13**, 2851–2865.

Stojanovic, M., Romanò, F. and Kuhlmann, H. C. (2022), 'Stability of thermocapillary flow in liquid bridges fully coupled to the gas phase', *J. Fluid Mech.* **949**, A5 (51pp).

Stojanović, M., Romanò, F. and Kuhlmann, H. C. (n.d.), '`MaranStable`: A linear stability solver for multiphase flows in canonical geometries', *SoftwareX* . Submitted.

Wanschura, M., Shevtsova, V. S., Kuhlmann, H. C. and Rath, H. J. (1995), 'Convective instability mechanisms in thermocapillary liquid bridges', *Phys. Fluids* **7**, 912–925.

Yano, T., Maruyama, K., Matsunaga, T. and Nishino, K. (2016), 'Effect of ambient gas flow on the instability of Marangoni convection in liquid bridges of various volume ratios', *Intl J. Heat Mass Transfer* **99**, 182–191.